

Institutionen för systemteknik

Department of Electrical Engineering

Examensarbete

Fuel Pressure Modelling in a Common-Rail Direct Injection System

Examensarbete utfört i Fordonssystem
vid Tekniska högskolan vid Linköpings universitet
av

Kurt Källkvist

LiTH-ISY-EX--11/4488--SE

Linköping 2011



Linköpings universitet
TEKNISKA HÖGSKOLAN

Fuel Pressure Modelling in a Common-Rail Direct Injection System

Examensarbete utfört i Fordonssystem
vid Tekniska högskolan i Linköping
av

Kurt Källkvist


LiTH-ISY-EX--11/4488--SE

Handledare: **Andreas Thomasson**
ISY, Linköpings universitet

Rikard Dyrsch
NESM, Scania CV AB

Examinator: **Lars Eriksson**
ISY, Linköpings universitet

Linköping, 17 August, 2011

	Avdelning, Institution Division, Department Division of Vehicular Systems Department of Electrical Engineering Linköpings universitet SE-581 83 Linköping, Sweden	Datum Date 2011-08-17
Språk Language <input type="checkbox"/> Svenska/Swedish <input checked="" type="checkbox"/> Engelska/English <input type="checkbox"/> _____	Rapporttyp Report category <input type="checkbox"/> Licentiatavhandling <input checked="" type="checkbox"/> Examensarbete <input type="checkbox"/> C-uppsats <input type="checkbox"/> D-uppsats <input type="checkbox"/> Övrig rapport <input type="checkbox"/> _____	ISBN _____ ISRN LiTH-ISY-EX--11/4488--SE Serietitel och serienummer ISSN Title of series, numbering _____
URL för elektronisk version http://www.vehicular.isy.liu.se http://www.ep.liu.se		
Titel Bränsletrycksmodellering i ett Common-Rail direktinsprutningssystem Title Fuel Pressure Modelling in a Common-Rail Direct Injection System Författare Kurt Källkvist Author		
Sammanfattning Abstract <p>The fuel pressure is one of the central control variables of a modern common-rail injection system. It influences the generation of nitrous oxide and particulate matter emissions, the brake specific fuel consumption of the engine and the power consumption of the fuel pump. Accurate control of the fuel pressure and reliable diagnostics of the fuel system are therefore crucial components of the engine management system. In order to develop for example control or diagnostics algorithms and aid in the understanding of how hardware changes affect the system, a simulation model of the system is desirable.</p> <p>A Simulink model of the XPI (Xtra high Pressure Injection) system developed by Scania and Cummins is developed. Unlike the previous models of the system available, the new model is geared towards fast simulations by modelling only the mean flow and pressure characteristics of the system, instead of the momentary flow and pressure variations as the engine rotates. The model is built using a modular approach where each module represents a physical component of the system. The modules themselves are based to a large extent on the physical properties of the components involved, making the model of the system adaptable to different hardware configurations whilst also being easy to understand and modify.</p>		
Nyckelord Keywords Fuel injection, Model, Simulation, Pressure, Common-Rail		

Abstract

The fuel pressure is one of the central control variables of a modern common-rail injection system. It influences the generation of nitrous oxide and particulate matter emissions, the brake specific fuel consumption of the engine and the power consumption of the fuel pump. Accurate control of the fuel pressure and reliable diagnostics of the fuel system are therefore crucial components of the engine management system. In order to develop for example control or diagnostics algorithms and aid in the understanding of how hardware changes affect the system, a simulation model of the system is desirable.

A Simulink model of the XPI (Xtra high Pressure Injection) system developed by Scania and Cummins is developed. Unlike the previous models of the system available, the new model is geared towards fast simulations by modelling only the mean flow and pressure characteristics of the system, instead of the momentary flow and pressure variations as the engine rotates. The model is built using a modular approach where each module represents a physical component of the system. The modules themselves are based to a large extent on the physical properties of the components involved, making the model of the system adaptable to different hardware configurations whilst also being easy to understand and modify.

Sammanfattning

Bränsletrycket är en av de centrala styrvariablerna i ett modernt common-rail insprutningssystem. Det påverkar utsläppen av kväveoxider och partiklar, motorns specifika bränsleförbrukning och bränslepumpens effektförbrukning. Noggrann reglering och tillförlitliga diagnoser av bränslesystemet är därför mycket viktiga funktioner i motorstyrsystemet. Som ett hjälpmedel vid utveckling av dessa algoritmer samt för att öka förståelsen för hur hårdvaruförändringar påverkar systemet är det önskvärt med en simuleringsmodell av bränslesystemet.

En Simulink modell av XPI (Xtra high Pressure Injection) systemet som utvecklats av Scania och Cummins har utvecklats. Till skillnad från de redan tillgängliga modellerna av systemet fokuserar denna modell på snabba simuleringsförlopp genom att enbart modellera medeltryck och medelflöden istället för de momentana trycken och flödena i systemet när motorn roterar. Modellen är uppbyggd av moduler som var och en representerar en fysisk komponent i systemet. Modulerna är mestadels uppbyggda kring de fysikaliska egenskaperna hos komponenten de försöker modellera vilket gör modellen av systemet anpassningsbar till olika hårdvarukonfigurationer och samtidigt lätt att förstå.

Acknowledgments

I would like to thank my supervisor here at Scania, Rikard Dyrsch, and my boss, Lars Eriksson, for giving me the opportunity to write this thesis and all the help and support they have provided during the process. I would also like to thank Thomas Timren at Cummins for sharing his extensive knowledge and experience in modelling the XPI system.

From ISY, I would like to thank my supervisor, Ph.D. student Andreas Thomason, and my examiner, Associate Professor Lars Eriksson, for their valuable opinions and remarks on my work.

Contents

1	Introduction	1
1.1	Overview	1
1.1.1	System Operation	1
1.1.2	Influences of Fuel Pressure on Engine Performance and Emissions	2
1.2	Purpose	3
1.3	Goals	3
1.4	Related Research	3
1.5	Suggested Solution	5
2	Modeling	7
2.1	Overview	7
2.2	Fluid Properties	7
2.3	Control Volume	8
2.4	Orifice Flow	9
2.5	Low Pressure System	9
2.5.1	Low Pressure Pump	10
2.5.2	Pressure Relief Valve	11
2.5.3	Inlet Metering Valve	12
2.6	High Pressure Pump	13
2.6.1	Inlet Check Valve	14
2.6.2	Outlet Check Valve	16
2.6.3	Pumping Chamber Volume	19
2.6.4	Pump Leakage	21
2.7	High Pressure System	24
2.7.1	Fuel injectors	25
3	Model Verification and Results	27
3.1	Overview	27
3.2	Low pressure system	27
3.3	High pressure pump	28
3.4	Complete system	29
3.5	Simulation Time	31

4 Discussion	37
4.1 Overview	37
4.2 Limitations of the Model	37
4.3 Suitable Applications	38
4.4 Suggested Improvements	38
4.5 Conclusion	39
Bibliography	41
A Derivation of the expression for the isothermal bulk modulus	45
B Schematic symbols	46
C Flow measurements from Rikard	47
D Stationary points for flow comparison	49
E Common abbreviations and denominations	50
E.1 Abbreviations	50
E.2 Denominations	50

Chapter 1

Introduction

1.1 Overview

The following section provides an introduction to the fuel injection system that is to be modeled within this thesis as well as some background to the influences of fuel injection pressure on the operation of a direct injection (DI) diesel engine.

1.1.1 System Operation

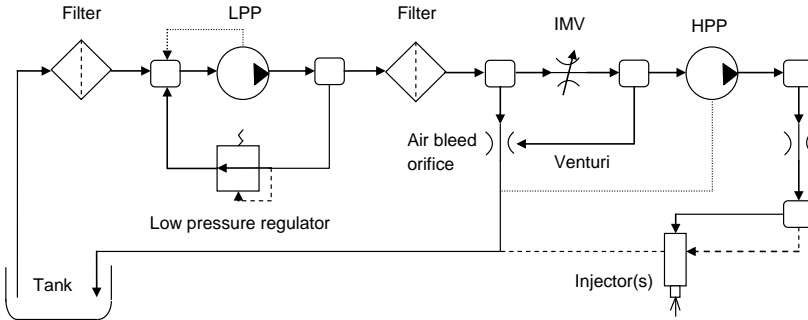


Figure 1.1. A basic flow schematic of the XPI-system excluding the mechanical dump valve since it should not contribute to the overall flow of the system during normal operation. See appendix B for symbol definitions.

The fuel injection system used by Scania is called XPI, Xtra high Pressure Injection, and is a so called Common Rail (CR) system developed by Cummins and Scania. A basic schematic of the system can be seen in figure 1.1. The system

consists of a low-pressure pump (LPP) that sucks fuel from the fuel tank through a filter and feeds it to the high-pressure pump (HPP) through another filter. The HPP pumps the fuel to the fuel rail, increasing the fuel pressure to 500-2500 bar depending on driving conditions. The fuel rail feeds the fuel to the injectors which inject it directly into the combustion chamber.

The fuel pressure in the fuel rail is controlled by varying the amount of fuel fed to the HPP from the LPP. This is accomplished using a so called inlet metering valve (IMV) fitted at the inlet of the HPP. The flow of the IMV is controlled by the engine management system (EMS) by applying a variable current to a solenoid in the IMV.

Between the second fuel filter and the IMV is a restriction that returns a small amount of fuel to the fuel tank. This is intended to bleed any entrained air from the system to ensure that no air bubbles can form in the HPP preventing it from building enough pressure or even damaging it. This restriction is also used to create a venturi effect [13] that sucks a small amount of fuel from the volume after the IMV. This is intended to make the system tolerant against small leakages through the IMV when it is closed by sucking out any fuel that leaks past the IMV and returning it to the fuel tank. Without this, any leakage past the IMV could result in rising rail pressure during overrun conditions when there is no fueling demand from the engine.

To protect the system from too high pressures in case of system malfunction the fuel rail is fitted with a mechanical dump valve (MDV) that is triggered if the fuel pressure exceeds 3100 bar. When the MDV is triggered it mechanically controls the fuel pressure to about 1000 bar and the vehicle can be driven to a workshop in limp-home mode.

1.1.2 Influences of Fuel Pressure on Engine Performance and Emissions

The fuel pressure is one of the central control variables in a CR DI system. As shown by Hountalas et al. [9] a high injection pressure is essential in reducing particulate matter (PM) emissions as well as the brake specific fuel consumption (BSFC) of a DI diesel engine. These improvements come at the cost of higher emissions of nitrous oxides (NO_x), higher peak cylinder pressure [9] and also an increase in pump power consumption [11] which indicates that careful control of the injection pressure plays an important role in the management of DI diesel engine. Unsurprisingly, both Bianchi et al. [2] and Woermann et al. [26] state that the injection rate of a CR injector is dependent on the pressure differential over the injector nozzle. Therefore, if variations in the fuel pressure at the injector are not accounted for, ensuring that the injected amount of fuel is the same as the commanded amount can be difficult.

Current and upcoming demands on vehicle emissions, noise and fuel consumption necessitate high injection pressures that can be rapidly and accurately controlled. To be able to evaluate upcoming hardware changes and test new control strategies

early in the development process it is desirable to have a model of the system upon which the changes can be tested.

1.2 Purpose

The purpose of the thesis is to develop a model of the fuel system and its components (LPP, IMV, HPP, fuel rail and injectors) in order to increase the understanding of how different hardware changes such as altered flow rates and different pressurized volumes influence the system. Another use of the model is to aid in the design of diagnosis and adaptation algorithms as well as provide an early test bench for new control strategies.

1.3 Goals

The goal of this thesis is to implement a MatLab/Simulink model of the fuel system that simulates the fuel pressure as a function of engine speed, commanded IMV position and fuel injection rate. The simulated railpressure should be within 10% of the actual rail pressure for any combination of engine speed, IMV position and fuel injection rate that is within the permissible limits of the engine.

The model should be suitable for simulating longer cycles, possibly tens of minutes, which effectively puts a limit on the minimum speed of the simulation. In order for the model to be usable for such long cycles, the time necessary for simulating the system should be no longer than 3-5 times the real time length of the cycle to be simulated, preferably faster. The model should also:

- Be adaptable to different engine configurations, such as different number of cylinders and different rail designs.
- Be user-friendly; a moderately skilled Matlab/Simulink user should be able to simulate the model on any computer with a working, current MatLab/-Simulink installation.

1.4 Related Research

In works such as Pump Handbook [11], Liquid Pipeline Hydraulics [13] and Fluid Power Engineering [15] the basics of hydraulics design, operating principles and modelling can be found. These works present the general relationships describing the pumping cycle of a piston type pump, the basic properties of fluids and their influence on the design and operation of a hydraulic system and the basic dynamics of liquid flows in pipes, hoses and various restrictions.

An often cited work in the field of hydraulic modelling is Fluid Transients [27]. It systematically describes several different modelling approaches such as lumped

element, transmission line and others based on the governing equations of motion and continuity. Pipe branching, pumps, valves and restrictions are described and analyzed and methods for controlling transients due to for example valve operations are derived.

More topic specific information can be found primarily in SAE-papers that present a substantial amount of research into the operation and dynamics of CR fuel injection systems.

In [17], Rodriguez-Anton et al. describe the variations of the physical properties of diesel (and common substitutes) due to changes in pressure and temperature. Fluid density, viscosity, isothermal compressibility (bulk modulus) and vapor pressure are investigated and expressions describing their dependency on pressure and/or temperature are presented.

Woermann et al. [26] have developed a model of a CR injection system for use in hardware-in-the-loop (HIL) simulations. They have used highly intuitive, relatively simple models for the CR system which they have divided into three parts, the pump, the injector and the fuel rail. The model simulates the dynamic characteristics of the fuel pressure and mass flow but disregards possible effects of fuel momentum. The end result is a model that correctly captures the main dynamic properties of the system (time-constants and overshoot during pressure transients) but appears to give a poor representation of the smaller oscillations produced by the pulsating flow of the pump and injectors. The model does however have the distinct advantage of being relatively computationally undemanding and intuitive to understand and modify.

In [4], Chiavola and Giulianelli used the AMESim environment to develop a model of a CR injection system. Once again the main components of the model are the pump, injectors and rail; however this model also includes the control system for the fuel injection. The model makes use of additional volumes to represent the connecting pipes between the components unlike the model by Woermann et al. [26]. The pump model is very similar to the one used by Woermann et al. but the injector model is more advanced attempting to model the different parts of the injector as opposed to just the basic flow-rate properties. The model of the rail and connecting pipe volumes is intended to model the damping effects of the components on the pressure fluctuations induced by the pump and injectors. Unfortunately the details about the different models are rather scarce as the paper focuses more on the simulation of a complete system consisting of both the CR system components as well as the control system.

Huhtala and Vilenius [10] used a model of a CR injection system to investigate the behavioral differences of two different rail configurations. They also investigated the influence of pressure on the bulk modulus, density and sonic speed of the fuel and applied their findings to the model. The model used is not described in great detail, but does make use of fluid transmission line methods to take into account inertial effects of the fluid. This is a common method for describing wave-propagation effects in radio frequency electronics which has proven useful within

the field of high-pressure hydraulics as well.

Although the work by Bianchi et al. [2] is focused on modelling and simulating a CR high-pressure injector in great detail, it does have certain merits when it comes to modelling a complete CR system as well. These merits stem mainly from the approach taken to represent the connecting pipes where continuity and conservation of momentum equations were used to describe the wave propagation in long pipes.

Teng and McCandless [24] present an interesting paper on the performance of CR rail-pressure supply pumps. They describe not only the performance and discharge characteristics at full load, but also the influence of inlet metering (pump throttling). They show that as the mean pump flow is decreased compared to the maximum flow capacity of the pump, the pressure oscillations due to the pump discharge increase. This phenomenon becomes more pronounced the fewer plungers the pump has since the overlapping between the discharge cycles of the different plungers decrease.

Hiroshi et al. [8] used an Optimized Finite Element Model (OFEM) to represent the pipe-segments of a CR injection system. The pump and injector models used were physical models based on force balance and flow rate equations. The use of OFEM to model the pipe segments enabled the authors to simulate the wave propagation in the pipes due to the injection events with a high degree of accuracy.

In [7], Ghazimirsaid et al. used the commercial software GT-FUEL [23, 12] to simulate the effects of different pipe dimensions on oscillations due to fuel injections in a CR injection system. The software uses a combination of one- and three-dimensional descriptions of the continuity, momentum and energy equations of the fluid to represent different object. A pipe for example is represented as a one-dimensional object whereas a flowsplit object uses a three-dimensional representation. The simulated results were in good agreement with measured data which indicates that the GT-FUEL software is a good tool for CR fuel system modelling.

GT-FUEL has been used by Cummins together with Scania to create detailed models of the components of the XPI system. These models will hopefully provide a valuable starting point when modelling the system and also prove useful when evaluating the model developed within the scope of this thesis.

1.5 Suggested Solution

Since the developed model should be adaptable to different engine configurations and hardware changes, the main approach to the modelling process will be physical modelling. The suggested structure of the model can be seen in figure 1.2. The pressure in the control volumes will be determined through the ratio between the mass of fluid in the volume and the volume of the container using the density and bulk modulus of the fluid. For most flow generating components the flow will

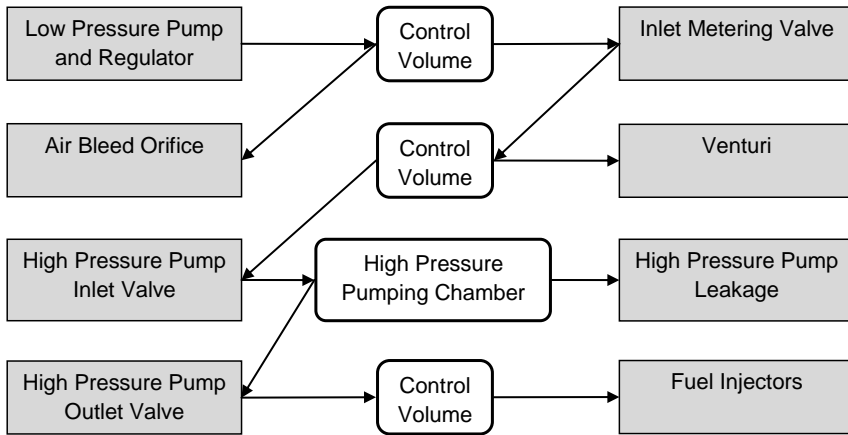


Figure 1.2. Overview of the suggested solution. Grey boxes indicate flow driving components and white boxes indicate pressure generating components; this is also indicated by the direction of the arrows.

be described as a function of the pressure difference between the adjacent control volumes and external control signals such as engine speed.

The key to success with this approach will likely be accurate modelling of the fuel flow and leakages of the different components, mainly the HPP and injectors. Because of the small pressurized volume and high stiffness of the liquid even small variations in the fuel flow can lead to very large pressure variations. In the initial model the elasticity of the fuel will be used to relate the fuel mass in the high pressure part of the system to the pressure - this will likely result in a stiff system since the dynamics of the elasticity are very fast compared to the rest of the system.

The MDV will not be included in this model at the present time since it should not contribute to the overall flow of the system under normal operation.

Chapter 2

Modeling

2.1 Overview

The system was modeled in three stages, each stage attempting to capture different physical parts of the system. The first stage dealt with the low pressure part of the system, the second the HPP and the third stage the high pressure parts such as the injectors and the fuel rail. The most difficult stage was the second one - two different modelling approaches were tried in order to find a model of the pump that could capture the fuel flow accurately enough with a sufficiently low computational burden.

Some components, such as the fluid, were necessary in all three stages of the modelling process. Since these components are used frequently, they are described in the first sections of this chapter.

2.2 Fluid Properties

Four different fluid properties are used in the modelling of the XPI-system. These are the mass density, isothermal bulk modulus, dynamic viscosity and vapor pressure of the fluid.

Both the density and the isothermal bulk modulus of the fluid are calculated through an equation of state developed by Kolade et. al. [12]. The equation of state describes the density of the fluid as a function of pressure and temperature according to equation (2.1).

$$\rho(p, T) = a_0 + \frac{(p + a_1T + a_2)^{a_3+1}}{a_3 + 1} + p(a_4T^{a_5} + a_6) + a_7\sqrt{T} \quad (2.1)$$

The coefficients, $a_0 - a_7$, for the equation of state have been fitted to measured data [3] for ISO4113 test fluid [6] using a function supplied with the GT-FUEL [23] software.

Differentiating equation (2.1) with respect to pressure at constant temperature, the isothermal bulk modulus can be calculated according to equation (2.2), see also appendix A. The bulk modulus describes the fluids relative change in volume when subjected to a change in pressure, its elasticity.

$$\beta(p) = \rho_0 \left(\frac{\partial p}{\partial \rho} \right)_T = \frac{\rho}{\left(\frac{\partial \rho}{\partial p} \right)_T} \quad (2.2)$$

The dynamic viscosity of the fluid describes the fluids internal resistance to flow. More formally it can be written as the ratio between the shear stress and the velocity gradient in a flow. For more information, see for example [1, 13, 15]. For this thesis, the dynamic viscosity of the fluid as a function of temperature and pressure is given by a table from [3].

Finally, the vapor pressure of the fluid is the lowest pressure at which the fluid will remain in its liquid phase at that temperature. Any further decrease in pressure will cause the fluid to spontaneously evaporate. The vapor pressure of the fluid can be described according to equation (2.3). The coefficients of the equation along with the equation have been found in the paper by Rodriguez-Anton et al. [17].

$$p_{\text{vapor}} = C_1 e^{\frac{C_2}{T}} \quad (2.3)$$

The fluid temperature used to determine the fluid properties described above is calculated though a second order polynomial function of pressure where the coefficients have been fitted to data from [3], see equation (2.4).

$$T(p) = a_2 p^2 + a_1 p \quad (2.4)$$

Equation (2.4) describes the isentropic increase in fluid temperature when the pressure is increased from an initial pressure to the final pressure p . By adding the result from equation (2.4) to the initial fluid temperature, the final temperature of the compressed fluid can be calculated.

2.3 Control Volume

Two different types of control volumes have been implemented, a simple one for volumes where the variations in pressure and temperature over time are assumed to be small and a more complicated one that handles large pressure variations. The difference between the two is that the simpler version assumes the fuel properties to be constant whilst the more complicated one uses equation (2.1) to estimate the fuel density and equation (2.2) for the bulk modulus of elasticity as a function of temperature and pressure.

For both types of control volumes the pressure is calculated in the same way. Using the definition of the bulk modulus of elasticity (see appendix A), the net mass flow

into the volume and the physical volume of the component the pressure can be calculated according to equation (2.5):

$$\begin{aligned} \frac{dp}{dt} &= \frac{\beta(p)}{-V(t)} \frac{dV}{dt} \Rightarrow p(t) = \int_0^t \frac{\beta(p)}{-V(t)} \frac{dV}{dt} dt \\ \frac{dV}{dt} &= \frac{dm}{dt} / \rho(p) + \frac{dV_{chamber}}{dt} \end{aligned} \quad (2.5)$$

2.4 Orifice Flow

Many flow generating components in the system have been represented by the generally accepted equation for incompressible flow through an orifice, equation (2.6). This equation can be derived from Bernoulli's equation by assuming steady state, incompressible, inviscid, laminar flow unaffected by gravity [13].

$$\frac{dm}{dt} = C * A \sqrt{2\rho(p_{upstream} - p_{downstream})} \quad (2.6)$$

C is the orifice flow coefficient and A is the cross sectional area of the orifice hole. If $p_{downstream}$ drops to the vapor pressure of the fluid, the flow through the orifice will not increase with a further decrease in downstream pressure. This is a situation known as choked flow.

2.5 Low Pressure System

The first components in the fuel flow path of the system are the fuel filters, low pressure pump, regulator valve, inlet metering valve, air-bleed orifice and venturi (see figure 1.1). The models for these components will be described and motivated in the following section.

The pressure in the low pressure part of the system is low (8-12 bar) and therefore all fuel properties such as bulk modulus of elasticity, density and viscosity have been assumed constant. Also, since the LPP has significantly more discharge cycles per engine revolution than the HPP, the flow of the LPP has been assumed to be steady, non-pulsating.

Both the air-bleed orifice and the venturi are modeled as fixed geometry restrictions discharging to atmospheric pressure according to equation (2.6). The orifice diameters are given by the physical dimensions of the holes while the discharge coefficient of both orifices is assumed to be about 0.6, a commonly used value for orifice plate flow coefficients where the orifice diameter is small compared to the diameter of the adjacent pipes.

The first of the two filters is also modeled as fixed geometry restriction, the effective flow area of this component has been determined by Cummins [25]. Unlike the other components of the model, this is a cross-coupling model that estimates

the outlet pressure of the filter as a function of the inlet pressure and flow rate. This is done by re-arranging the equation of orifice flow, equation (2.6), solving for $p_{downstream}$. The second filter is excluded from the model in order to make the simulations faster. This will cause a slightly higher pressure in the control volume before the IMV, however this difference does not appear to be significant as can be seen in section 3.2.

2.5.1 Low Pressure Pump

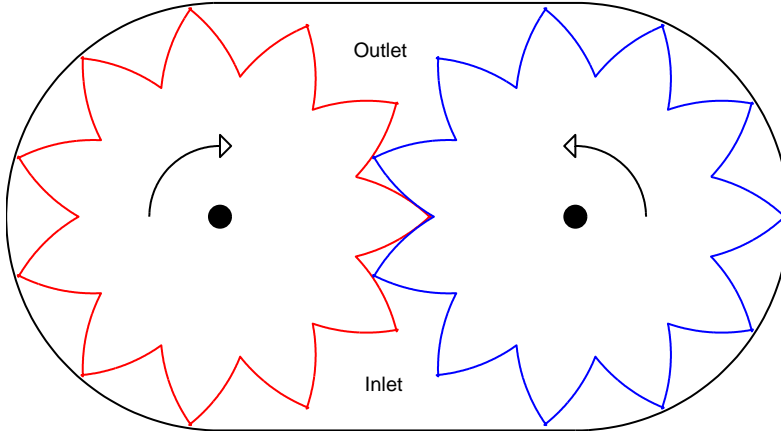


Figure 2.1. Drawing of a gear-type pump similar to the low pressure pump of the XPI system.

The low pressure pump is a gear-type pump consisting of two gears inside a chamber. The chamber fits tightly around the two gears which are meshed in the middle of the chamber, see figure 2.1. The pump will therefore pull fluid along the walls of the chamber in the direction of rotation and discharge the fluid as the gears mesh in the middle. The effect is a pump that displaces a fixed volume of fluid for every revolution, a volume which can be calculated knowing the dimensions of the gears.

By multiplying the total discharge per revolution with the number of revolutions per second of the pump and the fluid density, a linear relationship between mass flow rate and pump speed is found according to equation (2.7). The value for the pump discharge per revolution has been supplied by Cummins [25].

$$\frac{dm}{dt} = \rho * V_{LPP} * \frac{N}{60} \quad (2.7)$$

The flow from equation (2.7) is the theoretical maximum flow of the pump and thus has to be reduced to account for leakages past the gears and the small amount of fluid pumped in the wrong direction between the two gears as they mesh. This is accomplished using a gray box model with a constant term to represent the fluid

pumped between the gears whilst the leakage between the gears and the walls is modeled as a simplified plane Poiseuille flow between parallel plates [16]. The simplification is made by assuming that the length of the plates are equal to their width whereby the equation reduces according to equation (2.8). Thus, only the clearance between the plates and the constant leakage term have to be estimated which has been done by Cummins [25].

$$\frac{dm}{dt} = \rho \frac{W\delta^3\Delta p}{12\mu L} = \rho \frac{\delta^3\Delta p}{12\mu} \quad (2.8)$$

2.5.2 Pressure Relief Valve

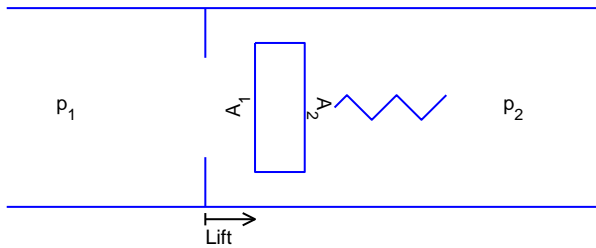


Figure 2.2. Drawing of the basic elements of a spring loaded valve.

The pressure of the low-pressure part of the fuel system is regulated by a mechanical relief valve that recirculates fuel from the high-pressure to the low-pressure side of the pump if the fuel pressure is high enough.

This valve is a simple spring loaded valve, see figure 2.2, whose motion can be described by considering the forces acting upon it. These forces consist of two major components, the spring force and the force from the difference in fuel pressure between the two sides of the valve. If the pressure force is large enough to overcome the spring pretension, the valve will open and let fuel flow past. The valve is assumed to be massless whereby the valve lift can be described by Hook's law according to equation (2.9) where k is the spring rate. As fuel flows past the valve, the fuel pressure differential over the valve will decrease and thus the pressure force will decrease causing the valve to close.

$$\text{lift} = \frac{A_1 p_1 - A_2 p_2 - \text{pretension}}{k} \quad (2.9)$$

The flow through the valve is described by the equation of flow through an orifice, equation (2.6), where the effective discharge area of the orifice is a function of the valve lift. The relationship between valve lift and effective discharge area is given by a table supplied by Cummins [25].

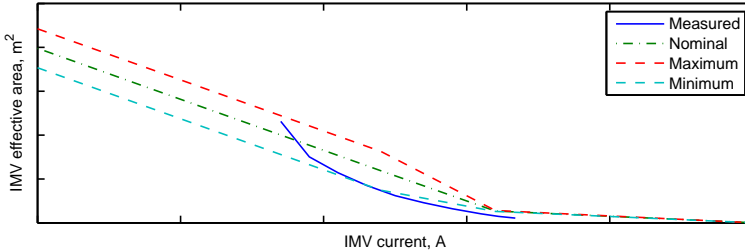


Figure 2.3. Effective discharge area of the IMV as a function of the applied current, both the measured values and the nominal curve with tolerances as given by the engineering drawing [22].

2.5.3 Inlet Metering Valve

The inlet metering valve consists of a spring-loaded valve connected to a solenoid. The spring holds the valve in the fully open position unless a current is applied to the coil of the solenoid whereby the magnetic force closes the valve. By varying the current to the solenoid, the magnetic force and thus the opening of the valve can be altered. The flow of the valve is described by the equation of flow through an orifice, equation (2.6), where the effective discharge area as a function of the current for the valve has been determined from measurement data.

Prior to the start of this thesis work, Rikard Dyrsch had performed a series of measurements in an injection test-cell in order to investigate the flow versus current characteristics of the IMV. The test-cell was equipped with a six-cylinder Scania engine without pistons, an electric motor to drive the engine and a measurement system. The measurement system was essentially six beakers placed on scales that collected all the fuel injected into each of the six cylinders during a defined period. When the period was over, the total change in mass of each of the beakers was recorded and the beakers were emptied to prepare for a new measurement. During these test, only five injectors were connected, the beaker for the sixth cylinder was instead used to measure the return flow from different parts of the system.

Two different sets of measurements were taken, the first one used the sixth scale to record the pilot leakage flow of the five fuel injectors, a small fuel flow that is used to control the opening of the injectors and then returned to the tank. The second one used the sixth scale to measure both the pilot leakage, the HPP leakage and the flow from the air-bleed orifice and the venturi. The collected data can be seen in appendix C.

The data collected by Rikard was unfortunately not enough to define the current-flow relationship of the IMV since the IMV-flow could not be isolated due to the flow through the air bleed orifice. Therefore, this data was used along with the model to estimate the effective flow area of the IMV for different currents. This was accomplished by simulating the model at each of the different stationary points (engine speed and rail pressure) used by Rikard with a range of different effective

areas for the IMV. The total flow through the system as measured by Rikard (see appendix C, Totalt flöde) was then compared to the total flow of the simulated system at that stationary point for all effective flow areas to find the effective flow area that gave the correct total flow. By taking the average of all the different calculated flow areas for a given current after removing the outliers the effective flow area as a function of current could be defined. The result can be seen in figure 2.3 along with the nominal curve from the engineering drawing [22].

2.6 High Pressure Pump

The most challenging part of the system to model has been the high pressure pump and its associated inlet and outlet check valves. Due to the large difference between the inlet and outlet pressures of the pump, the fluid properties and also the leakage vary greatly over the course of a pumping cycle which should be accounted for in order for the discharge rate of the pump to be correct.

The high pressure pump is a piston type pump with floating pistons called plungers. The plungers are floating in the sense that they are not physically connected to any other part, instead they are "floating" freely inside the barrel of the pumping chamber. This reduces the risk of cavitation inside the pumping chamber since the only force pushing the plungers down is the pressure force - if the pumping chamber pressure drops below the atmospheric pressure, the pressure force will push the plunger upwards thus hopefully preventing a further decrease in pressure that could cause cavitation. Due to the inertial effects of the plungers, cavitation can still occur however. During compression, the plungers are forced upwards by a camshaft with two lobes per plunger. At the pump inlets and outlets are check valves that prevent fluid from flowing from the high pressure to the low pressure parts of the system.

Scania uses two different HPP configurations, a two plunger HPP for inline five and six cylinder engines and a three plunger HPP for V8 engines. The HPP is driven at crankshaft speed, thus a two plunger HPP will have four discharge cycles for every engine revolution since the pump camshaft has two lobes for each plunger.

The HPP has been modeled using two different approaches. The first approach is very similar to the way the HPP was modeled by Cummins [25] and uses the laws of physics to describe the motion of the valves and plungers as the HPP cam rotates. This approach will henceforth be referred to as the cycle modelling approach since it models the motion of the different parts of the HPP over the course of a pumping cycle.

Due to the large forces and small masses and volumes involved, some dynamics of the system captured by this model are very fast necessitating a small simulation time step making the model computationally demanding. Therefore a second approach was employed to create a faster model more suitable for simulating longer time intervals. This approach disregards the pulsating nature of the pump flow and attempts to capture the time averaged flow rate of the pump over the course of a pumping cycle and will be referred to as the mean value model.

2.6.1 Inlet Check Valve

The inlet check valve, ICV, is a one way valve; its purpose is to let fluid in to the pumping chamber during the intake stroke of the plunger and not let it back out again during the compression stroke. The ICV is opened by the pressure force resulting from the pressure differential between the pumping chamber and the low pressure volume at the pump inlet during the intake stroke of the pump and is closed by a spring and the pressure force as the compression stroke of the pump causes the fluid pressure inside the pumping chamber to rise.

Cycle Model

The ICV is modeled as a flat, spring loaded flapper-valve, much like the low pressure regulator valve in section 2.5.2. Due to the pulsating flow characteristics of the high pressure pump, a more detailed motion model for the valve is used compared to the low pressure regulator valve. This motion model uses a mass to represent the valve and describes the motion of the valve through integration of the forces applied to it according to Newton's laws of motion, see equation (2.10). Almost the entire model of the cycle modelling ICV has been borrowed from the GT-FUEL model developed by Cummins [25].

$$\text{Lift}(t_1) = \frac{1}{m} \int_{t_0}^{t_1} \int_{t_0}^t F_{net}(\tau) d\tau dt \quad (2.10)$$

The forces acting upon the valve are the forces from the fluid pressure, the spring force and also the contact forces between the valve and the seat as well as between the valve and a physical stop at the maximum lift of the valve. The spring force is described by Hook's law with a constant spring rate and pretension whilst the net pressure forces are described by equation (2.11). This means that the outlet side pressure, p_2 , is assumed to be the only pressure acting in the area between the valve and the seat.

$$F_{pressure} = p_1 \frac{D_{bore}^2 - D_{rod}^2}{4} \pi - p_2 \frac{D_{bore}^2}{4} \pi \quad (2.11)$$

The contact forces are described as a combination of viscous damping and nonlinear spring forces which are applied as the valve body make contact with the seat or stop. This allows the valve body to penetrate the seat or stop by a small amount, this amount is negligible compared to the total stroke of the valve however.

When the valve is sufficiently close to the seat or stop and the separation between them is decreasing, a damping force proportional to the velocity of the valve body relative to the seat or stop is applied. When the separation between them is large enough or small but increasing, no damping is applied.

When the valve starts to penetrate the seat or stop, a spring force (not the linear spring force that always acts upon the valve) is applied according to Hook's law

where the spring rate or stiffness is described by equation (2.12) where x denotes the penetration depth and k the maximum contact stiffness. This ensures that the full contact stiffness is applied when the penetration is equal to or greater than the maximum penetration depth whilst providing a smooth transition from no contact stiffness.

$$\text{stiffness} = \left(k \left(\frac{\min(x, x_{max})}{x_{max}} \right)^2 \left(3 - 2 \left(\frac{\min(x, x_{max})}{x_{max}} \right) \right) \right) \quad (2.12)$$

The geometric area, A_{geom} , available for flow in the valve was calculated from the valve dimensions. The geometric area of the valve at any time is limited to the smallest of the throat area, A_{throat} , and the curtain area, $A_{curtain}$, as indicated in figure 2.4. The limitation is implemented by computing the critical lift of the valve as the lift where the curtain area is equal to the throat area, see equation (2.13). The geometric area of the valve is then calculated as the minimum of the actual curtain area and the curtain area at the critical lift.

$$A_{curtain}(\text{lift}_{crit}) = A_{throat} \Leftrightarrow \pi D_{bore} \text{lift}_{crit} = \frac{D_{bore}^2 - D_{rod}^2}{4} \pi \Leftrightarrow \quad (2.13)$$

$$\text{lift}_{crit} = \frac{D_{bore}^2 - D_{rod}^2}{4D_{bore}}$$

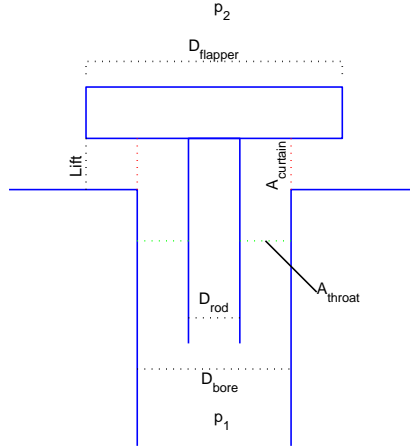


Figure 2.4. Drawing of the main components of the inlet check valve where the important dimensions are marked.

According to Gamma Technologies [23] who have developed the GT-FUEL software, the discharge coefficient of many hydraulic valves can be described by equation (2.14).

$$C_d = C_{d,max} \tanh \left(\frac{2\lambda}{\lambda_{crit}} \right) \quad (2.14)$$

λ denotes the flow number, a quantity that is similar to the Reynolds number [13] but uses the isentropic velocity instead of the actual fluid velocity. The flow number is calculated according to equation (2.15) where D_h denotes the hydraulic diameter which is calculated according to (2.16) where P_{wet} is the wetted perimeter.

$$\lambda = \frac{D_h}{\mu} \sqrt{2\rho |p_2 - p_1|} \quad (2.15)$$

$$D_h = \frac{4A_{geom}}{P_{wet}} = \dots = 2\text{lift} \quad (2.16)$$

Mean Value Model

The mean value modelling inlet check valve is described in a manner similar to its cycle modelling counterpart. The only difference between the two is that the mean value model assumes that the valve lift is always equal to the maximum valve lift and that the valve is a strict one way valve. This means that the valve is described by the equation of flow through an orifice, equation (2.6), where the pressure differential can never be negative. The discharge coefficient is described by the hyperbolic tangent function of the flow number, equation (2.14).

This model was motivated by the fact that the spring of the ICV is weak compared to the pressure forces, thus the valve is almost always fully open during the intake stroke. An example of this can be seen in figure 2.5.

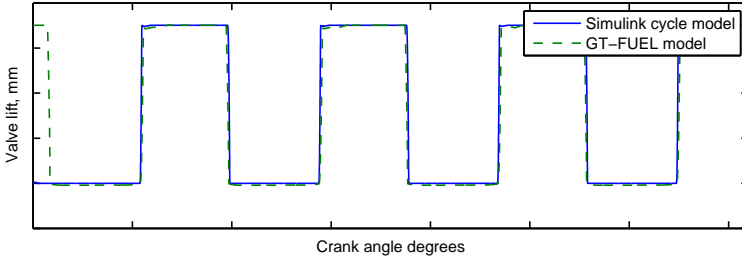


Figure 2.5. Simulated lift of the ICV during two crankshaft revolutions for both the Simulink model described in section 2.6.1 and the GT-FUEL model [25]. The lift very quickly reaches the maximum lift and is then nearly constant throughout the rest of the intake stroke. The system was operated at 1500RPM with a constant rail pressure of 1500bar and an IMV opening corresponding to 50% of the maximum effective flow area of the IMV.

2.6.2 Outlet Check Valve

The outlet check valve, OCV, performs the same task as the ICV in section 2.6.1 but on the outlet side of the HPP; it allows fluid to flow from the pumping chamber to the high pressure volume at the pump outlet, but not the other way. Just like

the ICV the OCV is a spring loaded, pressure operated valve. Almost the entire model of the cycle modelling OCV has been borrowed from the GT-FUEL model developed by Cummins [25].

Cycle Model

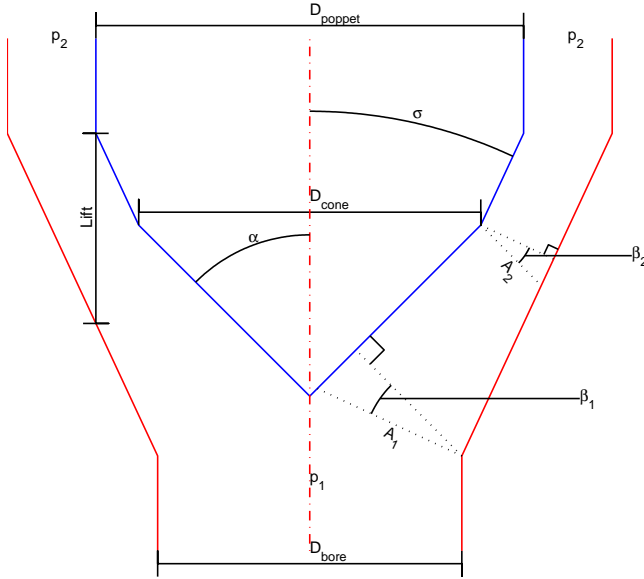


Figure 2.6. Drawing of an OCV valve with a double conical poppet and a conical seat.

The OCV is modeled in a manner similar to that of the inlet check valve. The main difference between the two is the way the effective discharge area is calculated. Since the outlet check valve is a conical poppet valve with a conical seat, see figure 2.6, the equations describing the discharge area are significantly more complicated than those of the ICV. The geometric area, A_{geom} , available for flow can be described by equation (2.17).

$$A_{geom} = \min(A_1, A_2, A_{throat}) \quad (2.17)$$

The throat area is described in the same way as for the ICV, see equation (2.18). Area A_1 is the area between the bottom of the seat and the lower part of the cone, see figure 2.6 as described by equations (2.19) to (2.22).

$$A_{throat} = \pi \frac{D_{bore}^2}{4} \quad (2.18)$$

$$A_1 = \frac{\pi D_{bore} (\text{lift} \sin \alpha + S_0)}{\cos \beta_1} \left[1 - \frac{\text{lift} \sin \alpha + S_0}{D_{bore}} (\cos \alpha + \sin \alpha \tan \beta_1) \right] \quad (2.19)$$

$$\tan \beta_1 = M_1 - \sqrt{M_1^2 - \frac{1}{2}} \quad (2.20)$$

$$M_1 = \frac{1}{4} \left[\frac{D_{bore} \sin \alpha}{\text{lift} \sin \alpha + S_0} \left(\frac{1}{\tan^2 \alpha} + 1 \right) - \frac{1}{\tan \alpha} \right] \quad (2.21)$$

$$S_o = \frac{(D_{cone} - D_{bore}) \cos \alpha}{2 \tan \sigma} (\tan \alpha - \tan \sigma) \quad (2.22)$$

Area A_2 is the area between the seat and the lowest part of the upper cone, see figure 2.6, as described by equations (2.23) to (2.25).

$$A_2 = \frac{\pi D_{cone} \text{lift} \sin \sigma}{\cos \beta_2} \left[1 + \frac{\text{lift} \sin \sigma}{D_{cone}} (\cos \sigma - \sin \sigma \tan \beta_2) \right] \quad (2.23)$$

$$\tan \beta_2 = M_2 - \sqrt{M_2^2 - \frac{1}{2}} \quad (2.24)$$

$$M_2 = \frac{1}{4} \left[\frac{D_{cone}}{\text{lift}} \left(1 + \frac{1}{\tan^2 \sigma} \right) + \frac{1}{\tan \sigma} \right] \quad (2.25)$$

Just as for the ICV in section 2.6.1 the discharge coefficient of the valve is calculated through a hyperbolic tangent function of the flow number, equations (2.14) and (2.15). Due to the complex geometry of the valve, in GT-FUEL [25] the hydraulic diameter was approximated according to equation (2.26).

$$D_h = \frac{4A_{geom}}{P_{wet}} \approx 2 \text{lift} \sin \alpha \quad (2.26)$$

Just like the ICV in section 2.6.1 the motion of the OCV is governed by Newton's laws of motion, also the spring and contact forces of the OCV are described in the same way as for the ICV. The pressure forces are described by equation (2.27).

$$\begin{aligned} F_{pressure} &= p_1 \frac{D_{cone}^2}{4} \pi + \frac{p_1 + p_2}{2} \frac{D_{poppet}^2 - D_{cone}^2}{4} \pi q(\text{lift}) - \\ & p_2 \frac{D_{cone}^2}{4} \pi - p_2 \frac{D_{poppet}^2 - D_{cone}^2}{4} \pi q(\text{lift}) \Leftrightarrow \\ & \Leftrightarrow (p_1 - p_2) \frac{D_{cone}^2}{4} \pi + \frac{p_1 - p_2}{2} \frac{D_{poppet}^2 - D_{cone}^2}{4} \pi q(\text{lift}) \end{aligned} \quad (2.27)$$

The function $q(\text{lift})$, defined by equation 2.28, essentially reduces the force produced by the pressure acting in the sealing area of the valve as the valve lift goes towards zero and applies the full force as the actual valve lift equals lift_{set} .

$$q(\text{lift}) = 1 - e^{(-3 \frac{2\text{lift}}{\text{lift}_{set}})} \quad (2.28)$$

Mean Value Model

The mean value model uses a bare minimal representation of the OCV. No flow characteristics are modeled, only the opening pressure of the valve is taken into account. This drastic simplification was necessary since the mean value model provides no real knowledge of the pressure inside the pumping chamber. Without such knowledge, a detailed model of the OCV is hardly useful. Instead, the time averaged flow of the OCV is assumed to be the flow of the ICV minus the pump leakage.

The opening pressure of the OCV is used to estimate the pressure of the pumping chamber at the end of the discharge stroke; this pressure is simply estimated as the pressure of the control volume downstream from the OCV plus the opening pressure, see equation (2.29), which can be derived from the equations in section 2.6.2. The opening pressure of the OCV has been defined as the pressure differential required to maintain the valve lift at the minimum lift where the full pressure force is applied to the seat area of the valve, thus $q = 1$ from equation (2.28). Knowledge of this pressure is necessary in order to estimate the inlet flow of the pump.

$$\begin{aligned}
 F_{spring} &= F_{pressure} \Leftrightarrow \\
 \Leftrightarrow p_{open} &= \frac{F_{spring}}{\frac{D_{cone}^2}{4}\pi + \frac{D_{poppet}^2 - D_{cone}^2}{8}\pi q} \Rightarrow \\
 \Rightarrow [q = 1] &\Rightarrow p_{open} = \frac{8F_{spring}}{(D_{cone}^2 + D_{poppet}^2)\pi}
 \end{aligned} \tag{2.29}$$

$$p_{chamber} = p_{outlet} + p_{open}$$

2.6.3 Pumping Chamber Volume

The pumping chamber is essentially a control volume capable of handling large pressure variations. These pressure variations stem from the change in chamber volume caused by the plunger as the cam rotates. In order to account for the motion of the plunger, the standard control volume, see section 2.3, has been extended with a motion model for the plunger and a cavitation model for the fluid.

Cycle Model

The motion of the plunger is described by Newton's laws of motion, similar to the way the motion of the ICV and OCV in sections 2.6.1 and 2.6.2 were described. The pump plunger is pushed down by the force from the pressurized fluid in the chamber and forced up by the contact force between the camshaft and the plunger.

The contact force is described in the same way as for the valves by viscous damping and a nonlinear spring, see section 2.6.1.

The pressure force acting upon the plunger is simply described as the product between the pressure differential over the plunger and its cross sectional area. The key feature to remember with regards to the pressure force over the course of a pumping cycle is that the volume of the pumping chamber when the plunger is at its top dead center position is significant. This means that even after the end of the discharge stroke, there will be a significant amount of compressed fluid in the chamber. As the plunger starts moving down, following the cam profile, the fluid will expand until it is at a low enough pressure for the ICV to open and let more fluid in. This means that for a portion of the decompression/filling stroke, the pressure in the chamber will be very high leading to a large force driving the plunger down. If the cam profile allows a high rate of plunger acceleration during this period, high plunger velocities can be reached giving the plunger a large momentum. This can cause the plunger to continue downwards even though the chamber pressure is low and thus not driving the plunger - if the ICV cannot let enough fluid through to maintain a chamber pressure above the vapor pressure of the fluid the fluid cavitates.

The control volume described in section 2.3 has been extended to account for cavitation as the average pressure of the fluid inside the chamber drops to the vapor pressure of the fluid. In case the fluid pressure in the pumping chamber drops to the vapor pressure of the fluid, the liquid equation of state, equation (2.1), cannot be used to describe the fluid properties. If that happens, the liquid will start cavitating which means that vapor pockets will start forming inside the chamber preventing the pressure from decreasing further until all liquid has turned to vapor. If all liquid has turned to vapor, the pressure in the chamber will be described by the ideal gas-law. The pressure in the pumping chamber is thus described by equation (2.30).

$$p(t) = \begin{cases} \int_0^t \frac{\beta(p)}{-V(t)} \frac{dV}{dt} dt & \text{if } \frac{\int_0^t \dot{m}_{net} dt}{\rho_{vapor}} \geq V(t) \\ \frac{RT \int_0^t \dot{m}_{net} dt}{MV(t)} & \text{if } \frac{RT \int_0^t \dot{m}_{net} dt}{Mp_{vapor}} \leq V(t) \\ p_{vapor} & \text{otherwise} \end{cases} \quad (2.30)$$

In equation (2.30) \dot{m}_{net} denotes the net mass flow rate into the pumping chamber, R denotes the universal gas constant, M is the average molar mass of the fluid and $V(t)$ is the volume of the pumping chamber at time t .

The first line of equation (2.30) can be recognized as the integral of equation (2.5) and describes the pressure in the chamber when all the fluid is in the liquid state. The second line can be derived from the ideal gas law and describes the pressure in the chamber when all the fluid is in a gaseous state. The last line states that if the fluid consist of a mixture of gas and liquid the pressure must be the vapor pressure of the fluid.

Mean Value Model

The pumping chamber of the mean value model is very different from the cycle modelling chamber. The task of the pumping chamber is to estimate the time averaged total flow of fuel into the pump during the course of a pumping cycle. This flow is assumed to be the smallest of the geometric flow and the ICV flow.

The ICV is described in section 2.6.1; it requires knowledge of the pressure in the pumping chamber in order to estimate the flow into the pump. This model uses the assumption that the flow from the ICV only limits the total flow into the pump when the fluid is cavitating inside the pump chamber, that is to say the pressure inside the pump chamber is the vapor pressure of the fluid or lower. In such cases the flow of the ICV is choked (see section 2.4) and therefore the pressure of the pumping chamber can be assumed to be the vapor pressure of the fluid. Finally, the ICV flow is scaled by the number of cylinders divided by two to account for the fact that each cylinder in the pump has its own ICV valve and also that the length of the intake stroke is approximately half the total length of the pumping cycle.

The geometric flow of the pump is described by equation (2.31) which takes into account both the geometry of the pump and the engine speed as well as the compressibility of the fluid.

$$\frac{dm}{dt} = \frac{NV_d \rho_{lp} n_r n_{cyl}}{60} \left(1 - \frac{\frac{\rho_{hp} V_c}{\rho_{lp}} - V_c}{V_d} \right) \quad (2.31)$$

$$V_d = \text{stroke} R_{plunger}^2 \pi \quad (2.32)$$

In equation (2.31), N denotes the pump speed in revolutions per minute, V_d the swept volume of one plunger as given by equation (2.32), n_r the number of strokes per revolution for one plunger, n_{cyl} the number of cylinders in the pump, V_c the compression volume of one pumping chamber and ρ_{lp} , ρ_{hp} the fluid density at ambient and pumping chamber pressure as described in section 2.6.2.

The rightmost term in equation (2.31) effectively reduces the mass of fluid the pump can take in during a revolution to account for the fact that part of the intake stroke of the pump is used to decompress the fluid trapped in the compression volume after the discharge stroke. As can be seen in the equation, this is accomplished by estimating the mass of the fluid trapped in the compression volume at the end of the discharge stroke and then calculating the volume this mass will occupy at ambient pressure. By subtracting the compression volume and then dividing by the swept volume, the ratio of the swept volume that is taken up by the decompression can be calculated.

2.6.4 Pump Leakage

Capturing the leakage of the HPP at different engine speeds, flow rates and outlet pressures has proven to be very challenging. The pressure and temperature variations affects both the fluid properties and the physical properties of the pumping

chamber; as the pressure also directly affects the flow rate and determines the temperature, the pressure dependency of the leakage is very complex.

Cycle Model

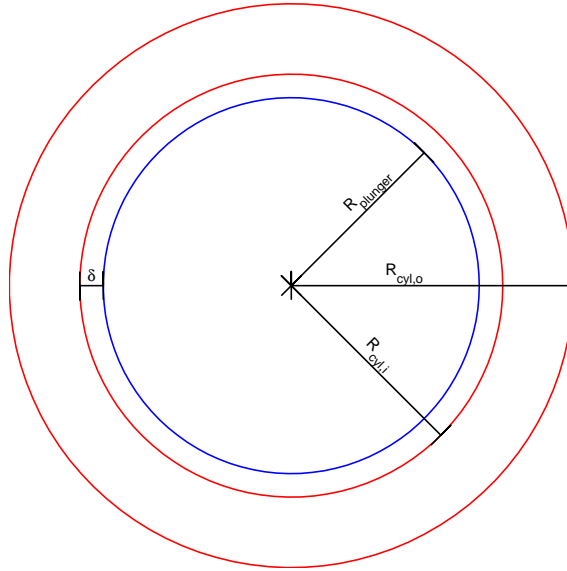


Figure 2.7. Drawing of a plunger surrounded by a pumping chamber where the different radii and the clearance are marked.

Assuming that the radius of the cylinder of the high pressure pump is much larger than the radial clearance between the plunger and the cylinder, the leakage past the plunger of the high pressure pump can be approximated as a combination of Poiseuille and Couette flow between parallel plates [16] according to equation (2.33) where the density is the mean density between the upstream and downstream pressures.

$$\frac{dm}{dt} = \rho\pi D\delta \left(\frac{\delta^2 \Delta p}{12\mu L} + \frac{1}{2} v_{plunger} \right) \quad (2.33)$$

D is the diameter of the plunger, $v_{plunger}$ is the velocity of the plunger relative to the barrel of the pumping chamber, L is the length through which the leakage occurs and δ is the radial clearance. Due to the geometry of the barrel, see references [21, 20], the leakage length can be described by equation (2.34) where $\text{pos}_{plunger}$ is the linear plunger position relative to bottom dead center.

$$L = \min(L_{max}, L_{min} + \text{pos}_{plunger}) \quad (2.34)$$

Due to the large variations in temperature and pressure during a pumping cycle, the radial clearance of the pump varies. This has been accounted for through

the use of the Lamé equations [19] that relates the variations in radial clearance to the variations in fuel pressure according to equation (2.35) which is actually a linear function of pressure. E denotes the Young's modulus of the material, ν denotes the Poisson ratio and R denotes the radius. The different subscripts *cyl* and *plunger* indicate that the property belongs to the cylinder or the plunger whilst the additional subscripts i and o indicate that the radius in question is the inner or outer radius of the component, see figure 2.7.

$$\Delta\delta(p) = \frac{pR_{cyl,i}}{E_{cyl}} \left(\nu_{cyl} + \frac{R_{cyl,o}^2 + R_{cyl,i}^2}{R_{cyl,o}^2 - R_{cyl,i}^2} \right) - \frac{pR_{plunger}}{E_{plunger}} (\nu_{plunger} - 1) \quad (2.35)$$

The temperature of the chamber walls and plunger also affect the radial clearance. The inner radius of the cylinder and the radius of the plunger are both assumed to obey the equation for linear thermal expansion [14], equation (2.36).

$$\Delta R = \alpha R \Delta T \quad (2.36)$$

$$\Delta\delta(T) = (\alpha_{cyl}R_{cyl} - \alpha_{plunger}R_{plunger}) \Delta T \quad (2.37)$$

α denotes the coefficient of linear thermal expansion for the material and ΔT the change in temperature from a nominal temperature. Since the cylinder and plunger are made from different materials, they have different coefficients of thermal expansion. The variation in radial clearance as a function of temperature can therefore be described by equation (2.37).

The temperature of the pumping chamber walls is assumed to be the same as the temperature of the fluid inside the chamber as described by equation (2.4). This is obviously a major simplification, but it should be a reasonable assumption at least for an infinitesimally thin layer of the chamber wall in contact with the fluid.

When approximating the leakage in the high pressure pump as Poiseuille-Couette flow, any eccentricity of the plunger will affect the effective radial clearance. Since the leakage flow rate is approximately proportional to the cube of the radial clearance (see equation (2.33)), the proper correction factor for calculating the effective radial clearance from the nominal clearance is found by integrating the cube of the clearance variation through a full circle and then taking the cube root. The clearance variation can be described by equation (2.38) which approximates to the final expression as the radii of the circles grow large compared to the nominal clearance.

$$\frac{d\delta}{d\alpha} = \varepsilon \cos(\alpha) + \sqrt{R_{cyl,i}^2 - \varepsilon^2 \sin^2(\alpha)} - R_{plunger} \approx \varepsilon \cos(\alpha) + 1 \quad (2.38)$$

$$\varepsilon = \frac{x_{cyl,i} - x_{plunger}}{R_{cyl,i} - R_{plunger}} \quad (2.39)$$

The ratio of eccentricity, ε , is described as the ratio between the offset of the centers of the circles and nominal clearance, see equation (2.39). The offset of the centers of the circles is described in one dimension by the difference $x_{cyl,i} - x_{plunger}$ where x denotes the position of the center of the circle indicated by the subscript.

The final expression for the clearance correction factor can thus be written as in equation (2.40).

$$f = \sqrt[3]{\frac{1}{2\pi} \int_0^{2\pi} (\varepsilon \cos(\alpha) + 1) d\alpha} = \sqrt[3]{1 + \frac{3\varepsilon^2}{2}} \quad (2.40)$$

Since the clearance factor is multiplied with the nominal clearance to create the effective clearance, at fully eccentric conditions, $\varepsilon = 1$, the leakage flow rate will increase about 2.5 times compared to fully concentric conditions.

The eccentricity ratio of the plunger is determined through a function of plunger velocity and pressure where higher pressure or higher velocity decreases the eccentricity. This function has been developed by Cummins [25], see equation (2.41).

$$\varepsilon = \sqrt{1 - \min\left(1, \frac{v_{plunger}^2}{9}\right) e^{\frac{-p}{2E^9}}} \quad (2.41)$$

Mean Value Model

Since the cycle modelling approach has knowledge of the pressure of the pumping chamber at all times, a detailed description of the pump leakage as a function of engine speed, pump flow and pressure can be used as shown in section 2.6.4. Without knowledge of the momentary pumping chamber pressure, using such a model has proven too difficult within the timeframe of this thesis. Therefore a simple linear leakage model has been fitted to measured data from appendix C using a least squares method. The leakage of this model is described by equation (2.42).

$$\frac{dm}{dt} = a_1 I_{IMV} + a_2 N + a_3 p_{outlet} + a_4 \quad (2.42)$$

I_{IMV} denotes the IMV current, N the engine speed in revolutions per minute and p_{outlet} the outlet pressure of the HPP.

2.7 High Pressure System

The high pressure side of the fuel system consists of a fuel line from the HPP to the fuel rail, an orifice, the fuel rail, injectors and the MDV, see section 1.1.1. As mentioned in section 1.5 the MDV will not be included in the model, thus only the fuel line, orifice, fuel rail and injectors will be modeled.

The fuel line and rail are modeled as control volumes with fluid properties that depend on the fuel temperature and pressure, see section 2.3. The orifice is described by the equation of flow through an orifice, equation (2.6) from section 2.4. The fluid properties in this component depend on the temperature and pressure of the fluid in the volume upstream of the orifice.

2.7.1 Fuel injectors

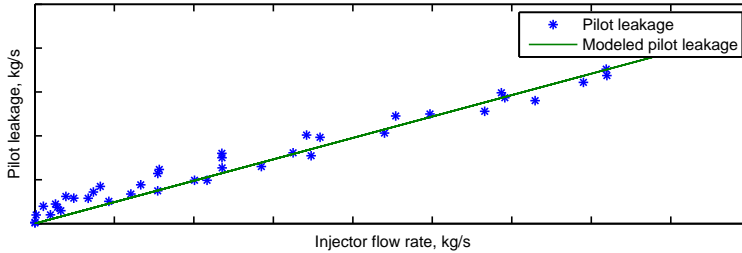


Figure 2.8. The actual and modeled pilot leakage as a function of injector flow rate. The linear approximation of the leakage appears to be a good representation of the actual pilot leakage.

The fuel injectors contribute two different flows to the system, as can be seen in figure 1.1. The flow rate of the injectors is a function of the rail pressure and thus for a given rail pressure the amount of fuel injected into the engine can be controlled by adjusting the time during which the injector is flowing. This is accomplished by applying a current from the engine management system to a solenoid in the fuel injector. This opens a small pilot valve which causes a pressure drop in a small volume called the control chamber inside the injector. As this pressure drops, a pressure differential is developed across the top of the injector needle causing a pressure force that lifts the needle allowing fuel to flow into the engine. As the current is released, the pilot valve closes and the pressure differential disappears allowing a return spring to seat the injector needle again stopping the flow of fuel [18].

The time averaged fuel flow into the engine can be described by multiplying the amount of fuel injected every time one injector opens by the number of injections per second. This flow is found through reverse table lookup using a map of the required injection time as a function of rail pressure and desired fuel amount. The number of injections per second can be found by multiplying the engine speed with the number of injectors and dividing by the number of revolutions per injection for one injector, see equation (2.43) where N is the engine speed in revolutions per minute, n_r is the number of revolutions per injection for one injector and n_{inj} is the number of injectors. This equation assumes that all injections during a cycle are the same length which is mainly useful when only one injection per cylinder per cylinder cycle is used. When modelling multiple injections, such as pre-, main- and post-injections, one injector block per injection type can be used. This approach can also be used for modelling different injectors for different cylinders if suitable parameters are chosen.

$$\frac{\text{injections}}{\text{second}} = \frac{Nn_{inj}}{60n_r} \quad (2.43)$$

The flow through the pilot valve is called the pilot leakage and is returned to the fuel tank instead of being injected into the engine. This flow is simply modeled

as a percentage of the injected fuel flow which is a fairly good approximation, especially for higher flow rates. The percentage of the injected flow is calculated by a least squares fit to measured data from appendix C. The result can be seen in figure 2.8.

Chapter 3

Model Verification and Results

3.1 Overview

In the following sections data will be presented in order to evaluate the accuracy and speed of the different models developed in section 2.

3.2 Low pressure system

The main purpose of the model of the low pressure system is to generate the pressure in the control volume upstream of the ICV. That pressure is generated by the fluid flow through the IMV and other flows; since the flow through the IMV is a function of the pressure upstream of the IMV it is important that the pressure is correct. Unfortunately no direct measurement data was available for that pressure, instead the model developed by Cummins [25] was used as a reference. That model is accurate to within 5% of actual measured data from a test rig at Cummins (e-mail correspondance with Thomas Timren, 2011-02-10). The comparison between the two models can be seen in figure 3.1.

As can be seen in figure 3.1 the mean pressure before the IMV of the Simulink model is accurate to within 4% of the GT-FUEL model from Cummins [25]. Since the flow of many components is described by the equation of orifice flow, equation (2.6), the flow errors resulting from the pressure errors of the low pressure part of the system should be smaller than 5% (the square root of the maximum accumulated pressure error of the two models).

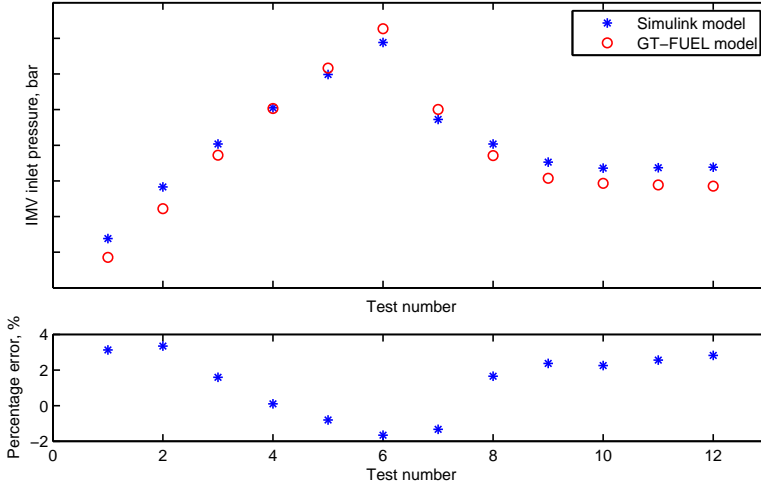


Figure 3.1. Simulated pressure before the IMV from the GT-FUEL model developed by Cummins [25] and the Simulink model developed within this thesis as described in section 2.5. The average pressure of the Simulink model is within 4% of that of the GT-FUEL model. The operating points used for the tests are described in appendix D.

3.3 High pressure pump

Due to the lack of measurement data, some results of the cycle modelling HPP have only been compared to the model from Cummins [25]. In figures 3.2, 3.3, 3.4 and 3.5 the pumping chamber pressure, ICV and OCV flow rates and pump leakage as a function of the crank shaft angle relative to the initial position are compared for the GT-FUEL model from Cummins and the cycle modelling Simulink model.

In figure 3.2 it can be seen that the Simulink model fails to capture the peak pressure and the rapid pressure fluctuations around the peak pressure. The most important features such as the rate of pressure buildup and drop off as well as the pressure drop when the OCV is open does seem to be captured fairly accurately though. Just like for the pumping chamber pressure, the ICV flow rate seen in figure 3.3 fails to capture the rapid variations in flow when the valve is open but appears to capture the average flow rate and the time the valve is open correctly. In figure 3.4 the differences between the Simulink and GT-FUEL models can clearly be correlated to the difference in pumping chamber pressure from figure 3.2. The valve opens at the correct time, misses the rapid flow fluctuations the rapid pressure fluctuations of the GT-FUEL model gives rise to and then captures the decreasing flow rate of the valve as the pressure in the pumping chamber drops.

The leakage flow rate of the HPP from the Simulink model as seen in figure 3.5 shows a larger discrepancy compared to the GT-FUEL model than the other flows

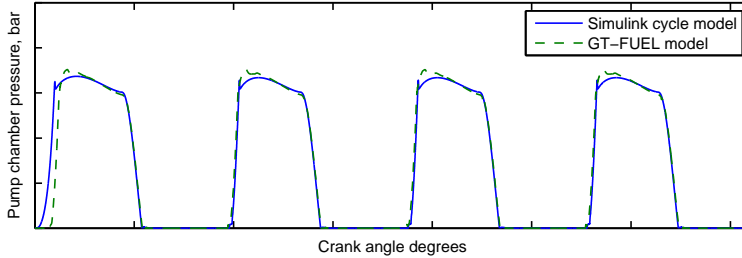


Figure 3.2. Simulated pump chamber pressure from the GT-FUEL model developed by Cummins [25] and the Simulink model developed within this thesis as described in section 2.6.3. The Simulink model accurately captures the compression and decompression parts of the pumping cycle, but underestimates the pumping chamber pressure at the very beginning of the discharge stroke. The system was operated at 1500RPM with a constant rail pressure of 1500bar and an IMV opening corresponding to 50% of the maximum effective flow area of the IMV.

described previously. The length of the part of the cycle where the leakage is large is captured accurately as would be expected since the fuel pressure is the main factor for determining the leakage and the compression and decompression are accurately captured. The leakage during the part of the cycle where the fuel pressure is high is not captured very accurately though, most likely due to differences in how the radial clearance varies with temperature and pressure between the two models.

The time averaged HPP inlet fuel flow for the GT-FUEL, cycle modelling Simulink and the mean value modelling Simulink models can be seen in figure 3.6. As can be seen in the figure, the mean value model actually performs better than the cycle model; however both models show results that are within 1% of the GT-FUEL model except when the flow rate approaches zero in test number seven.

The leakage of the mean value model was modeled by a linear function of pressure, engine speed and IMV current as shown in section 2.6.4. In figure 3.7 the resulting leakage is compared to the measured data from appendix C. The leakage flow rate shows the largest percentage of error of all the modeled flows and even though the total leakage flow is small compared to the total flow of the pump the actual error in the leakage flow is of the same order of magnitude as for example the error in the average inlet flow rate. This makes it a significant contributor to the total flow rate error and therefore a prime candidate for improvement.

3.4 Complete system

Once a complete model of the system had been assembled it was tested by stimulating it with engine speed, injection time and IMV current data from tests performed in an injection test rig. First the stationary points from appendix C were used to test the system over a broad spectrum of operating points. The results can be

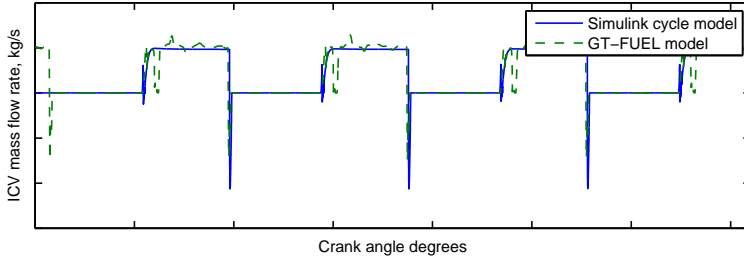


Figure 3.3. Simulated ICV flow for one valve from the GT-FUEL model developed by Cummins [25] and the Simulink model developed within this thesis as described in section 2.6.1. The Simulink model appears to capture the main characteristics of the ICV flow, but misses some oscillations as the valve opens. The system was operated at 1500RPM with a constant rail pressure of 1500bar and an IMV opening corresponding to 50% of the maximum effective flow area of the IMV.

seen in figure 3.8; several of the tested operating points result in a simulated rail pressure more than 10% lower or higher than the true pressure. The worst point results in a rail pressure about 15% higher than the true pressure and another four are at or just outside the 10% limit.

Several dynamic tests were also performed where the engine speed and IMV current were fixed and the injection time was altered in steps. Since this meant running the system in open loop without a rail pressure regulator, care had to be taken to choose combinations of injection times, IMV currents and engine speeds that resulted in rail pressures that were within the permissible limits. In figure 3.9 the resulting rail pressure is plotted along with the measured rail pressure from the test rig for such a test where the engine speed was fixed at 2000rpm and the IMV current at 0.9A giving a fairly high total mass flow rate. In order for the time constant of the model to accurately mimic the true time constant of the system, the volume of the fuel rail had to be increased by 5 times.

In figure 3.10 the step response of the system in a low flow situation at 1000rpm and an IMV current of 1.6A is shown. In both the high and low flow situations from figures 3.9 and 3.10 the step response time of the simulated system seems to agree well with the measured data once the rail volume had been increased. The accuracy of the modeled stationary pressures seems to vary a great deal depending on the operating point of the system however.

In figure 3.11 it can be seen that also for decreasing rail pressures the time constant of the model with an increased rail volume seems to agree well with the measured data.

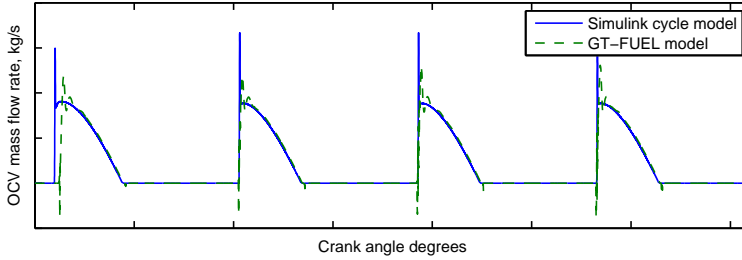


Figure 3.4. Simulated OCV flow for one valve from the GT-FUEL model developed by Cummins [25] and the Simulink model developed within this thesis as described in section 2.6.2. Just as for the ICV the Simulink model appears to capture the main flow characteristics of the valve, only missing some of the oscillatory behavior as the valve opens. The system was operated at 1500RPM with a constant rail pressure of 1500bar and an IMV opening corresponding to 50% of the maximum effective flow area of the IMV.

3.5 Simulation Time

The simulation time for the model using both the cycle modelling and the mean value modelling HPPs has been evaluated. This was done by simulating the systems at different stationary operating points for a short period of time at each point and then dividing the mean time taken to simulate the system by the length of the simulation. The result is a number describing the number of second it takes to simulate every second in real time, the speed of the simulation. The results are presented in table 3.1.

Table 3.1. Simulation speed for the two models

Model	Simulation speed, s/s	Tested cycle length, s	Average simulation time, s
Mean Value	<2	0.5	0.888
Cycle	>2000	0.08	193

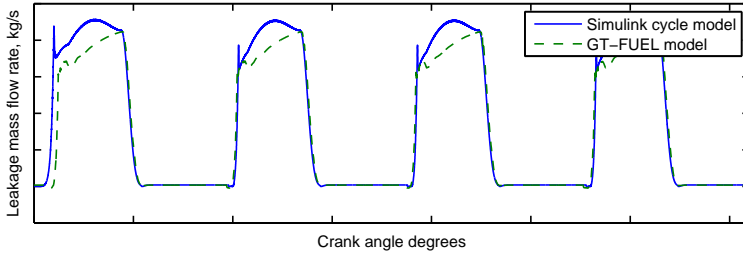


Figure 3.5. Simulated pump chamber leakage for one chamber from the GT-FUEL model developed by Cummins [25] and the Simulink model developed within this thesis as described in section 2.6.4. The flow difference between the two models during the discharge part of the pumping cycle is most likely due to the difference in how the radial clearance of the pumping chamber varies with temperature and pressure for the two models. The system was operated at 1500RPM with a constant rail pressure of 1500bar and an IMV opening corresponding to 50% of the maximum effective flow area of the IMV.

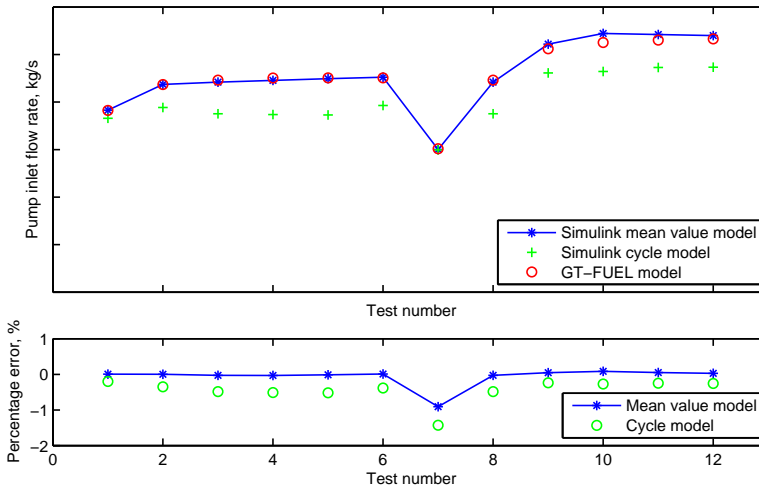


Figure 3.6. Time averaged HPP inlet flow rate from the GT-FUEL model developed by Cummins [25] and the mean value and cycle modelling Simulink models developed within this thesis. The pump inlet flow rate of the Simulink model very closely mimics the flow rate of the GT-FUEL model - the mean value model performs within one percent of the GT-FUEL model in all the tested operating points. The operating points are described in appendix D.

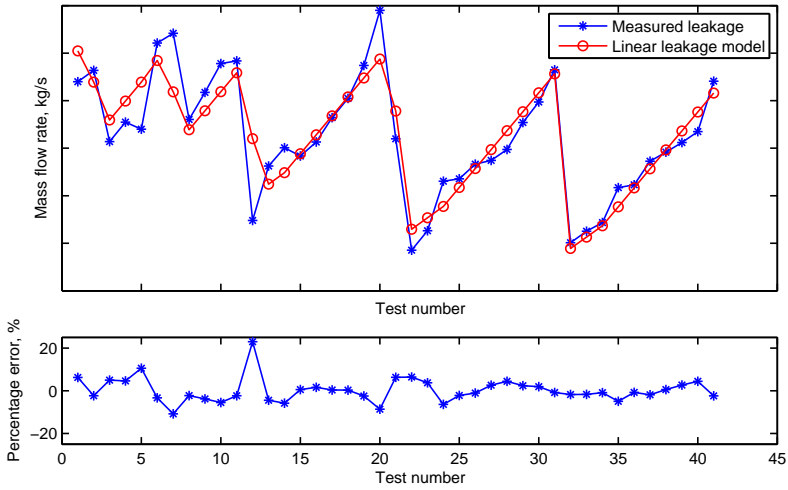


Figure 3.7. The leakage flow rate of the linear leakage model compared to the measured data from appendix C. Relating the figure to the used operating points from appendix C, it can be seen that the linear model is fairly accurate in capturing leakage variations as a function of different IMV currents, but less suitable for modelling leakage variations as a function of engine speed and rail pressure.

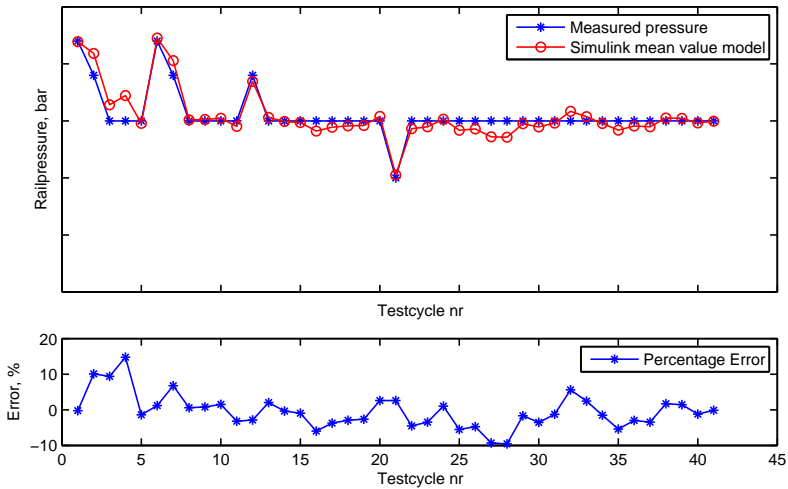


Figure 3.8. The measured and simulated rail pressure for the different stationary points specified in appendix C. Several of the operating points result in rail pressures more than 10% higher or lower than the true rail pressure.

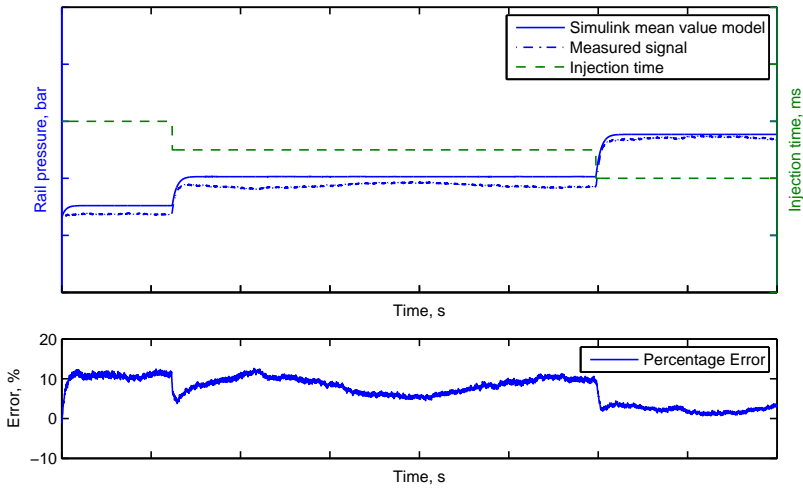


Figure 3.9. The measured and simulated rail pressure during injection time steps at 2000rpm and 0.9A IMV current. The time constant of the system is captured well by the model with an increased rail volume, but the model overestimates the stationary pressures slightly.

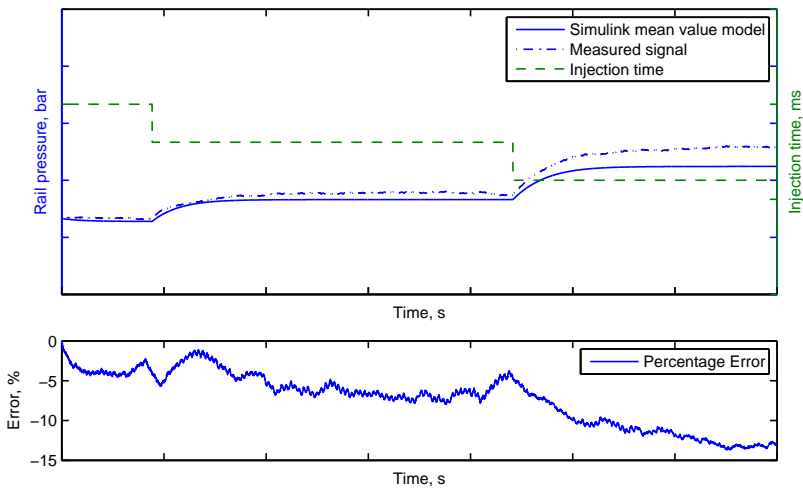


Figure 3.10. The measured and simulated rail pressure during injection time steps at 1000rpm and 1.6A IMV current. Once more the time constant of the model with an increased rail volume agrees well with the real system, but at these operating points the stationary pressures are underestimated.

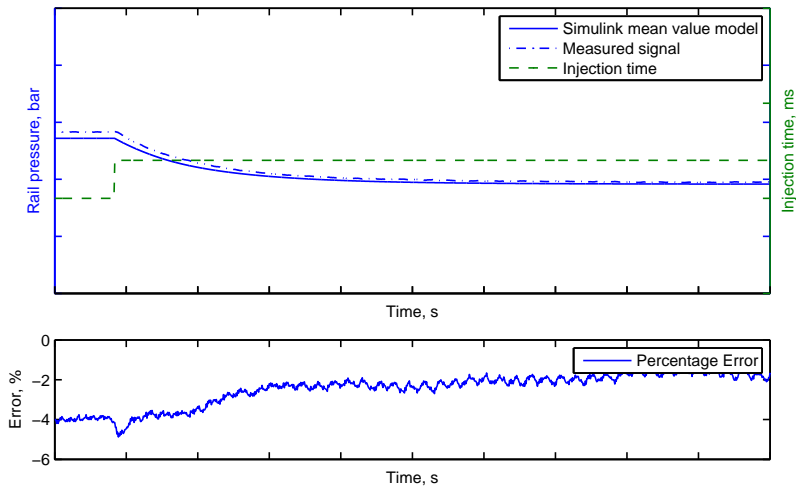


Figure 3.11. The measured and simulated rail pressure during one injection time step at 1000rpm and 1.6A IMV current. Also for falling rail pressures the time constant of the model with an increased rail volume agrees well with the real system, but once more the stationary pressures are slightly underestimated.

Chapter 4

Discussion

4.1 Overview

In the following sections, some of the limitations and their causes, the models suitability for different applications and possible improvements will be briefly discussed. The results of the developed model will also be related to the goals set forth in chapter 1.3.

4.2 Limitations of the Model

The current-flow area curve of the IMV, figure 2.3, imposes a severe limitation on the range of IMV currents that can be used in the model. With the available data, the entire permissible range of IMV currents could not be mapped to an effective flow area - for IMV currents outside the mapped range, linear extrapolation is used to estimate the effective area. This will most likely introduce large errors in the effective area of the IMV if the current is far outside the mapped range of currents.

The fact that the available data could not be used to isolate neither the IMV flow nor the leakage flow meant that the models for these component had to be fitted with the help of modeled flows. This means that there is a dependency between the IMV curve and the model of the low pressure system as well as between the leakage model and the low pressure system model and IMV curve. This limits the adaptability of the model to new hardware configurations - for example, changing the IMV would include not only measuring the flow area versus current relationship of the new IMV, but also fitting new coefficients for the leakage model.

Since the MDV is not included in the model, the model can obviously not be used for simulations that requires that component. Except for the actual modelling of an MDV, adding such a component to the system would not be difficult though.

4.3 Suitable Applications

Since the time constant of the model can be made to agree with measured data with relative ease, the model should be suitable for testing rail pressure control algorithms and other features that are dependent upon the time constant of the system. This could for example include high pressure leakage diagnosis or diagnosis and adaptation of large injector flows.

Due to the apparent difficulty in capturing the stationary pressure in different operating points, this model should not be used in applications where the precision of the stationary levels is important. Such applications could include virtual rail pressure sensors and possibly diagnosis algorithms.

The model makes no attempt at capturing the periodic variations of the rail pressure due to the oscillating flow of the pump and injectors or standing wave phenomenon in the rail. The model is therefore unsuitable for any applications where such behaviors are of interest, for such applications the GT-FUEL model from Cummins [25] might be used instead.

4.4 Suggested Improvements

As mentioned in section 3.3, the linear leakage model is a prime candidate for improvement since it displays a large error relative to the total leakage flow. The actual flow error is also large enough to make it among the larger of all the flow errors, thus reducing the leakage flow error percentage from the current $\approx 20\%$ (figure 3.7) of the total leakage in the worst operating points to a level similar to that of the HPP inlet flow rate (figure 3.6) would make a significant difference in the total flow rate error.

An initial attempt at improving the linear leakage model could be to look at the cycle modelling leakage model and from that try to determine a more suitable model order for the linear model than the currently used first order model. Fitting coefficients to a higher order model would however require more data than currently available. It would also be desirable to fit the coefficients of the model directly to measured data instead of the currently used data that has been biased by other parts of the model in order to improve the ease with which different components of the system can be changed.

Another possible improvement of the mean value leakage model would be to make it a physical model like the cycle modelling version. This would allow the model to take into account the properties of different fuels and different types of HPPs without having to run extensive test cycles to fit the coefficients of the current model making the model more easy to adapt to changes. It could also make the model more useful for developing certain features such as virtual fuel quality sensors that use the fuel properties to estimate what type of fuel that is currently being used.

The method by which the current versus flow area curve of the IMV was determined and also the actual range of currents it was determined for leaves room for improvement. If measurement data with pressures before and after the IMV, the flow through the IMV and the current was available for the entire permissible range of IMV currents an IMV curve could be generated that depends on the IMV only and not the entire low pressure system as is the case with the currently used curve. This could increase the range of IMV currents that can be used in the model as well as improve the ease with which the type of IMV can be changed in the model.

As mentioned in section 3.4, the volume of the fuel rail had to be increased by 5 times in the model in order for the time constant to be accurate. Even though making that change in the model is easy and the results seem to agree well with measured data, it should not be necessary. The model of a control volume, see section 2.3, is the main element responsible for the time constant of the complete model - this model only requires three parameters, the volume of the component and the bulk modulus and density of the fluid. Since the volume of the component is well defined by its physical dimensions, any error stemming from the control volume model is therefore likely to be caused by the fluid properties. Since it is unlikely that the bulk modulus or the mass density of the fluid are wrong by a factor of 5, it would seem that the fluid properties are not responsible for the erroneous time constant. Therefore the complete system should be re-examined in order to try and identify any further components that can introduce time constants.

4.5 Conclusion

The goal of the thesis as set forth in section 1.3 was to develop a model of the XPI system that could simulate the rail pressure as a function of engine speed, commanded IMV position and fuel injection rate. Such a model has been developed using a physical modelling approach to a large extent, unfortunately the simulated rail pressure does not meet the goal of being within 10% of the actual rail pressure in all permissible operating points of the engine. Out of 41 tested stationary operating points, one results in a rail pressure that is 15% too high and another four are at or slightly above the 10% limit. The remaining 36 points meet the requirement. When tested against dynamic rail pressure data the system displays similar performance with a maximum deviation of about 15%.

The time necessary for simulating the developed mean value model is about two times the real time length of the cycle to be simulated which makes the model suitable for simulating longer sequences. The cycle model is significantly slower, the time needed to simulate the system is about 2000 times longer than the cycle that is to be simulated. This makes the cycle model unsuitable for any simulations of sequences longer than a few crank shaft revolutions.

The developed model was created using a modular, physical modelling approach which means that it should be highly adaptable to different hardware configurations. Unfortunately, the parameters used to describe some of the components are

dependent upon other components in the model making some parts of the system more difficult to change than others; for example changing the IMV would require a measuring and fitting new coefficients to the leakage model.

The model requires only three external stimuli to run, engine speed, IMV current and injection time, and should therefore be relatively simple to run. The modular structure of the model should also make it intuitive to understand and modify.

By properly measuring the current versus flow area relationship of the IMV and improving the leakage model, the accuracy of the model and also the adaptability to new hardware configurations could be improved. The model should also be examined in order to figure out why the step response of the system is too fast when using the correct dimensions of certain components.

Bibliography

- [1] Arthur Akers, Max Gassman, and Richard Smith. *Hydraulic Power System Analysis*. CRC Press, 2006. ISBN 978-0-8247-9956-4.
- [2] G. M. Bianchi, S. Falfari, M. Parotto, and G. Osbat. Advanced modelling of common-rail injector dynamics and comparison with experiments. In *SAE Paper 2003-01-0006*. SAE International, 2003.
- [3] Bosch. Bränsle egenskaper bosch. File: X:\Engine_Dev\40_Engineering_Dev\SimulDoc\modeller\insprutning\Fuel-data\Bransle_egenskaper_Bosch.xls, 2011-05-23.
- [4] O. Chiavola and P. Giulianelli. Modeling and simulation of common-rail systems. In *SAE Paper 2001-01-3183*. SAE International, 2001.
- [5] International Organization for Standardization. Fluid power systems and components – graphic symbols and circuit diagrams – part 1: Graphic symbols for conventional use and data-processing applications. URL: http://www.iso.org/iso/iso_catalogue/catalogue_tc/catalogue_detail.htm?csnumber=43237, 2011-05-16.
- [6] International Organization for Standardization. Road vehicles – calibration fluids for diesel injection equipment. URL: http://www.iso.org/iso/iso_catalogue/catalogue_tc/catalogue_detail.htm?csnumber=50636, 2011-05-09.
- [7] A. Ghazimirsaid, M. Shahbakhti, and C. R. Koch. Study of the impact of system characteristics on pressure oscillations in a common-rail diesel fuel injection system. In *SAE Paper 2005-01-0910*. SAE International, 2005.
- [8] Akiyama Hiroshi, Yuasa Hiroyuki, Kato Akira, Saiki Toshinori, Sanada Kazushi, and Kado Naoki. Precise fuel control of diesel common-rail system by using ofem. In *SAE Paper 2010-01-0876*. SAE International, 2010.
- [9] D. T. Hountalas, D. A. Kourmenos, K. B. Binder, V. Schwarz, and G. C. Mavropoulos. Effect of injection pressure on the performance and exhaust emissions of a heavy duty di diesel engine. In *SAE Paper 2003-01-0340*. SAE International, 2003.

- [10] Kalevi Huhtala and Matti Vilenius. Study of a common-rail fuel injection system. In *SAE Paper 2001-01-3184*. SAE International, 2001.
- [11] Igor Karassik, Joseph Messina, Paul Cooper, William Chaplis, and Frederic Buse. *Pump Handbook*. McGraw-Hill Professional Publishing, 2007. ISBN 978-0-415-32717-6.
- [12] Badajide Kolade, Michael E. Boghosian, P. S. Reddy, and Shawn Gallagher. Development of a general-purpose, thermal-hydraulic software and its application to fuel injection systems. In *SAE Paper 2003-01-0702*. SAE International, 2003.
- [13] Shashi E. Menon. *Liquid Pipeline Hydraulics*. CRC Press, 2004. ISBN 978-0-8247-5317-7.
- [14] Carl Nordling and Jonny Österman. *Physics Handbook for Science and Engineering*. Studentlitteratur, 2007. ISBN 978-9-144-04453-8.
- [15] Galal M. Rabie. *Fluid Power Engineering*. McGraw-Hill Professional Publishing, 2009. ISBN 978-0-071-62606-4.
- [16] Durgaiiah Rama D. *Fluid Mechanics and Machinery*. New Age International Publishers, 2004. ISBN 81-224-1386-2.
- [17] L. M. Rodriguez-Anton, J. Casanova-Kindelan, and G. Tardajos. High pressure physical properties of fluids used in diesel injection systems. In *SAE Paper 2000-01-2046*. SAE International, 2000.
- [18] Scania. Xpi info. Document name: \\global\DFS04\Engine_Dev\15_Projects\Green_arrow_projects\CR\XPI\Scania info, utbildn\Aktuell XPI systempresentation\XPI info.ppt, 2011-05-25.
- [19] B Sundström. *Handbok och formelsamling i hållfasthetslära*. Institutionen för hållfasthetslära, KTH, 1999.
- [20] Cummins Fuel System. High pressure pump plunger engineering drawing. Cummins component part no. 4984606.
- [21] Cummins Fuel Systems. High pressure pump barrel engineering drawing. Cummins component part no. 4984182.
- [22] Cummins Fuel Systems. Inlet metering valve engineering drawing. Cummins component part no. 2872550.
- [23] Gamma Technologies. Gamma technologies - engine and vehicle simulation. URL: www.gtisoft.com, 2011-02-09.
- [24] Ho Teng and James C. McCandless. Performance analysis of rail-pressure supply pumps of common-rail fuel systems for diesel engines. In *SAE Paper 2005-01-0909*. SAE International, 2005.

-
- [25] Thomas Timren. Gt-fuel 2-cylinder high pressure pump model. File: pp201.gtm, 2011-02-10.
- [26] R. J. Woermann, H. J. Theuerkauf, and A. Heinrich. A real-time model of a common-rail diesel engine. In *SAE Paper 1999-01-0862*. SAE International, 1999.
- [27] Benjamin Evan Wylie and Victor Lyle Streeter. *Fluid Transients*. McGraw-Hill, 1978. ISBN 978-0-070-72187-6.

Appendix A

Derivation of the expression for the isothermal bulk modulus

Start with a general expression for the density of the fluid as a function of pressure and temperature and use a Taylor expansion in two variables to write:

$$\begin{aligned}\rho &= f(p, T) \\ &\approx \rho_0 + \left(\frac{\partial \rho}{\partial p}\right)_T (p - p_0) + \left(\frac{\partial \rho}{\partial T}\right)_p (T - T_0) \\ &= \rho_0 \left[1 + \frac{1}{\rho_0} \left(\frac{\partial \rho}{\partial p}\right)_T (p - p_0) + \frac{1}{\rho_0} \left(\frac{\partial \rho}{\partial T}\right)_p (T - T_0) \right] \\ &= \rho_0 \left[1 + \frac{1}{\beta} (p - p_0) + \alpha (T - T_0) \right]\end{aligned}$$

Assuming constant temperature, the equation simplifies to:

$$r = \rho_0 + \frac{\rho_0}{\beta} (p - p_0)$$

From the equation above, it is clear that the density of the fluid increases as the pressure increases - this and the definition of density allows us to write:

$$\frac{\rho_0}{\partial \rho} = -\frac{V_0}{\partial V}$$







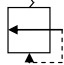

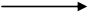
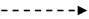
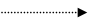
The minus indicates that the density increases as the volume decreases (assuming the mass remains constant). Using this we can derive the definition of the isothermal bulk modulus as used in this thesis:

$$\beta = \rho_0 \left(\frac{\partial p}{\partial \rho}\right)_T = -V_0 \left(\frac{\partial p}{\partial V}\right)_T$$

Appendix B

Schematic symbols

The schematic symbols presented below are based upon the ISO 1219-1:2006 [5] standard.

	Closed fluid accumulator/tank
	Vented fluid accumulator/tank
	Injection valve
	Fixed geometry restriction
	Variable geometry restriction
	Filter
	Mechanical pressure regulating valve
	Fixed displacement pump
	Normal flow connector
	Pilot/control flow connector
	Leakage/drain flow connector

Appendix C

Flow measurements from Rikard

The measurements were carried out in one of the fuel injection test-cells at Scania. The test-cell was equipped with a 6-cylinder engine running a 5-cylinder software calibration thus disabling the sixth injector. The fuel injection hardware used during the test can be seen in table C.1.

The fuel flow was measured by gathering all the injected fuel from the 5 injectors in 5 beakers place on scales over a period of time. At the end of the period the increase in mass of the beakers was recorded before the beakers were emptied to prepare for the next test. A sixth beaker and scale was used to measure the return flow from different parts of the system. First only the pilot leakage of the five injectors was measured, after that the tests were repeated and the total return flow of the system was measure.

The tests were carried out by specifying an engine speed and rail pressure and then manually adjusting the injection time until the desired IMV current was reached. Once the desired IMV current was reached, the fuel flow was measured and recorded.

Table C.1. Fuel injection hardware used for testing

Part:	Article nr:
Haldex Itasca low pressure pump	1947377
High pressure pump with 13mm stroke	1947373
XPI 235 Ver5 fuel injectors	1916167
Inlet Metering Valve	2024377

Testfall	Ontid ms	IMV Ström A	Varvtal RPM	Ralltryck bar	Totalt flöde g/s	Totalt returflöde g/s	Totalt spridflöde g/s	Pilotläckageflöde g/s
1	0,108	1,610	500	2200	9,22	9,25	0,02	0,01
2	0,441	1,550	500	1900	10,58	9,60	1,18	0,20
3	1,923	1,450	500	1500	14,21	9,45	5,16	0,51
4	3,429	1,350	500	1500	17,80	10,03	8,47	0,75
5	4,976	1,250	500	1500	21,68	10,78	11,81	0,99
6	0,119	1,610	700	2200	9,77	9,77	0,03	0,03
7	0,489	1,550	700	1900	11,93	10,19	1,92	0,29
8	1,759	1,450	700	1500	16,17	9,96	6,71	0,67
9	3,158	1,350	700	1500	20,44	10,70	11,03	0,99
10	4,660	1,250	700	1500	25,42	11,45	15,55	1,30
11	5,718	1,150	700	1500	29,30	12,19	18,92	1,55
12	0,181	1,670	1200	1900	8,68	8,22	0,27	0,20
13	0,410	1,610	1200	1500	10,36	8,99	1,80	0,37
14	0,639	1,550	1200	1500	12,64	9,45	3,93	0,58
15	1,046	1,450	1200	1500	16,59	9,98	7,54	0,88
16	2,064	1,350	1200	1500	21,78	10,66	13,05	1,27
17	2,956	1,250	1200	1500	26,82	11,40	17,85	1,61
18	4,166	1,150	1200	1500	33,25	12,21	24,06	2,06
19	5,417	1,050	1200	1500	40,46	13,21	30,86	2,56
20	6,053	0,950	1200	1500	45,11	14,23	34,27	2,80
21	8,311	0,850	1200	1000	48,23	13,60	37,73	3,22
22	0,351	1,670	1900	1500	9,13	8,34	1,74	0,45
23	0,439	1,610	1900	1500	10,77	8,70	3,02	0,58
24	0,532	1,550	1900	1500	13,05	9,43	4,40	0,72
25	0,852	1,450	1900	1500	17,68	10,20	6,88	1,14
26	1,215	1,350	1900	1500	22,34	10,86	13,27	1,50
27	2,005	1,250	1900	1500	28,00	11,51	19,90	1,97
28	2,866	1,150	1900	1500	34,82	12,33	27,35	2,50
29	3,456	1,050	1900	1500	41,86	13,16	32,43	2,87
30	4,318	0,950	1900	1500	49,33	14,03	39,36	3,38
31	5,283	0,850	1900	1500	57,80	15,17	46,92	3,99
32	0,217	1,670	2300	1500	8,88	8,46	0,93	0,39
33	0,380	1,610	2300	1500	10,57	8,83	2,57	0,62
34	0,523	1,550	2300	1500	12,92	9,22	4,97	0,85
35	0,766	1,450	2300	1500	17,27	10,29	9,06	1,23
36	1,019	1,350	2300	1500	22,76	10,85	13,36	1,60
37	1,516	1,250	2300	1500	28,18	11,66	19,11	2,02
38	2,094	1,150	2300	1500	34,69	12,37	25,15	2,45
39	2,789	1,050	2300	1500	41,62	13,17	32,32	2,98
40	3,521	0,950	2300	1500	49,58	13,98	39,46	3,52
41	4,308	0,850	2300	1500	57,95	15,20	47,49	4,08

Appendix D

Stationary points for flow comparison

The stationary points described in table D.1 were used for comparing the Simulink model developed within this thesis with the GT-FUEL model developed by Cummins [25].

Table D.1. Stationary operating points for model comparison.

Testcase	IMV area %	Engine speed RPM	Rail pressure bar
1	20	500	1500
2	20	1000	1500
3	20	1500	1500
4	20	2000	1500
5	20	2500	1500
6	20	3000	1500
7	0	1500	1500
8	20	1500	1500
9	40	1500	1500
10	60	1500	1500
11	80	1500	1500
12	100	1500	1500

Appendix E

Common abbreviations and denominations

E.1 Abbreviations

The following abbreviations will be used in this thesis:

CR - Common Rail

DI - Direct Injection

EMS - Engine Management System

HPP - High Pressure Pump

ICV - Inlet Check Valve

IMV - Inlet Metering Valve

LPP - Low Pressure Pump

MDV - Mechanical Dump Valve

OCV - Outlet Check Valve

E.2 Denominations

The following denominators will be used in the equations in this thesis:

A - Area

β - Isothermal bulk modulus

C - Flow coefficient

D - Diameter

δ - Clearance

E - Young's modulus

F - Force

I - Current

k - Spring rate

L - Length

m - mass

N - Rotational velocity

n_{cyl} - Number of cylinders

n_r - Number of cycles per revolution

P - Perimeter

p - Pressure

ρ - Mass density

R - Radius

T - Temperature

μ - Dynamic viscosity

V - Volume

v - Linear velocity

ν - Poisson ratio

W - Width